"ANALOG EXPERIMENTS OF LAVA FLOW EMPLACEMENT "

Einat Lev[1,*], Elise Rumpf[2], Hannah Dietterich[3]

[1] Lamont–Doherty Earth Observatory, Columbia University, New–York, NY, USA
[2] US Geological Survey, Astrogeology Science Center, Flagstaff, AZ, USA
[3] US Geological Survey, Alaska Volcano Observatory, Anchorage, AK, USA

ABSTRACT

Laboratory experiments that simulate lava flows have been in use by volcanologists for many years. The behavior of flows in the lab, where "eruption" parameters, material properties, and environmental settings are tightly controlled, provides insight into the influence of various factors on flow evolution. A second benefit of laboratory lava flows is to provide a set of observations with which numeri–cal models of flow emplacement can be tested. Models of lava flow emplacement vary in mathematical approach, physical assumptions, and computational cost. Nonetheless, all models require thorough testing and evaluation, and laboratory experiments produce an ex–cellent test for models.

This paper provides a primer on modern analog laboratory lava flow experiments. It reviews scaling considerations and provides quanti–tative information meant to guide future experimentalists in designing their experiments to be relevant to natural processes. Traditional and novel laboratory techniques are described, including a discussion of current limitations. New insights from recent experiments high–light the impact of topographic conditions and highlight the importance of considering bed roughness, major obstacles, and slope breaks. The influence of episodic or non–uniform effusion rate is demonstrated through recent experimental works. Lastly, the paper discusses sev–eral open questions about lava flow emplacement and the ways in which future improvements in experimental methods, such as the abil–ity to utilize three–phase suspensions and materials with complex rheologies and to image the interior of flows could help answer these.

1. MOTIVATION

Lava flows present a hazard to infrastructure and hu–man lives, as demonstrated recently by flows in Hawai'i [Patrick et al., 2017], Cape Verde [Jenkins et al., 2017] and elsewhere. At the same time lava flows cover vast areas on Earth and other planets and moons, and there–fore record a long history of planetary evolution and tectonic processes [e.g., Wilson and Head, 1983; Head et al., 1992]. Deciphering the factors that control how lava flows form and evolve [e.g., Manga and Ventura, 2005; Harris et al., 2016] is key to understanding these landscapes.

After many years of scientific study of lava flow em–placement, the basic understanding of the controlling factors has been established: Lava flow paths depend on the ground slope, the rheology of the lava, and the cool–ing conditions [e.g., Griffiths, 2000]. These factors have consequently been included in numerical flow models, the key tools used to assess lava flow hazard [e.g., Bilotta et al., 2016; Cappello et al., 2015; Harris et al., 2016; Hidaka et al., 2005; Kelfoun and Vargas, 2015; Tarquini et al., 2010]. However, there are still many as–pects of flow behavior that are observed in nature but are not currently included in simulation models. These include processes such as flow inflation and breakout, levee and channel formation, and the interaction of flows with bed roughness or vegetation. Many existing

simulation models also do not consider the impact of non–constant effusion rate, the impact of turbulence, or thermal or mechanical erosion of the substrate.

One of the popular means for shedding some light on these standing questions is through laboratory experiments that simulate flow emplacement by using analogous materials such as wax, paraffin, syrup, clay slurries, and, recently, molten basalts. Laboratory models of lava flow emplacement serve three main goals:

1. Provide intuition on the influence of specific factors on the flow, by systematically varying parameters and inferring an empirical behavior law that represents their influence

2. Produce well–controlled and calibrated data sets that can be utilized to test numerical flow models, which are then used to simulate flow emplacement in realistic conditions

3. Offer scaled and controlled environment for testing and training with instruments and techniques to be deployed and utilized in the field

This paper explains the considerations that go into designing laboratory flow experiments, reviews some of the classic works and results and insights gained from recent work, and outlines remaining limitations and challenges.

2. DESIGNING LABORATORY LAVA FLOW EXPERIMENTS

Analog laboratory flows and natural lava flows operate on different time and length scales. When designing a laboratory analog for lava flows, a scientist should consider the controlling forces (some of which may not be known or well understood yet), the important time and length scales, the feasibility and safety of the experimental procedure, and the available facility, tools and budget. The following sections address these requirements by discussing: Scaling of analog experiments to nature through dimensional analysis (Section 2.1), commonly used materials (Section 2.2) and tools and techniques (Section 2.3).

2.1 SCALING

A well–known method of ensuring that experiments capture the behavior of interest is through the use of *non-dimensional numbers*. Each of these numbers represents a ratio between the forces, time and length scales that control the flow. If a ratio is smaller than a

specific threshold, the flow will be within a specific regime; it will be in another regime if it is greater than that threshold. For example, a ratio greater than 1 points to dominance of one process, and if that same ratio is smaller than 1, another process dominates. The goal when designing an experiment is to strive to keep the non–dimensional numbers in the laboratory such that the experiment is in the same regime they have in nature. This ensures that the behaviors observed in the laboratory are relevant to the natural world despite the very different size, duration, and materials. For example, a highly turbulent flow in the lab will be a poor analog for a laminar natural flow and vice versa. Investigators can prevent this mismatch by noticing that the Reynolds number, the non–dimensional number that determines the level of turbulence, is different between the two systems. Similarly, a laboratory material that is strongly elastic on the experiment timescale will be a poor analog for a natural material that behaves viscously on the relevant timescale, and this can be avoided by looking at the systems' Deborah number.

The mathematical principle of the "Pi theorem" [Buckingham, 1914] states that a system with N parameters (e.g., flow length, liquid temperature, extrusion rate) and p fundamental units ((e.g., meter, second, kilogram, degree), can be described by N–p relationships between its parameters. These relationships are the so-called non–dimensional numbers. A recent review paper by Merle [2015] includes a detailed discussion on scaling between experiments and volcanic systems, including the fundamentals of dimensional analysis and similarity. Merle [2015] provide examples of scaling of experiments pertinent to pyroclastic flows and volcanic explosions, thus emphasizing brittle behavior and dilute suspensions. A short discussion of scale factors and dimensional analysis is also given by Kavanagh et al. [2018] as part of their review of experimental and numerical models in volcanology. This paper focuses on the scaling considerations most relevant for lava flow emplacement simulations. It introduces the mathematical definition of these numbers, and provides values for the relevant physical constants that construct them, to calculate typical ranges of the numbers for experiments and natural systems. Table 1 provides the definitions, units and typical values for material properties and conditions relevant for scaling of analog laboratory lava flow models. The following list gives a more detailed description of several non–dimensional numbers relevant to analog models of lava flows: The Péclet

Parameter	Symbol	Units	Dimensions	Typical values for Basalt flows	Typical values for Ryholite flows	Syrup	PEG 600	Molten basalt
Flo thickness	D	m	L	1–20	10 to 100	10^{-3} to 10^{-2}	10^{-2} to 10^{-1}	10^{-2} to 10^{-1}
Flow speed	U	m/s	L/T	0.01–20	3E-05	10^{-3} to 10^{-2}	10^{-4} to 10^{-3}	10^{-3} to 10^{-2}
Strain rates	$\dot{\varepsilon}$	1/s	1/T	10^{-4} to 20	$< 10^{-5}$	10^{-2} to 10^{-1}	10^{-2} to 10^{-1}	10^{-2} to 10^{-1}
Thermal diffusivity	κ	m²/s	L2/T	10^{-7} to 10^{-6}	5.5×10^{-7}	1.9×10^{-7}	8.16×10^{-8}	10^{-6}
Density	ρ	kg/m³	M/L³	500–2500	1900–2600	1400	1120	2800
Viscosity	η	Pa s	M/LT	10^{-2} to 10^{2}	10^{8} to 10^{12}	10^{-1} to 1	10^{-1}	10 to 10^{2}
Yield stress	σ_y	Pa	M/LT²	10 to 10^{4}	10^{4} to 10^{5}	0	40	0

ND number		Definition	Meaning					
Peclet number	Pe	UL/κ	Advection versus Conduction	10^{3} to 10^{8}	10^{8}	1500	312.5	300
Reynolds number	Re	ρ U L / η	Advection versus viscosity (turbulent / laminar)	1 to 2,000 Laminar to transitional	$<10^{-7}$ Laminar	2 to 5 Laminar	0.1 to 10 Laminar	10^{-4} to 10^{-4} Laminar
Flow regime parameter	Ψ	ts / ta	Advection versus solidification	Full range	Full range	NA (not solidifying)	Full range	> 2000
Deborah number	De	tr/to	Relaxation time versus Observation time	Mostly De << 1	Mostly De << 1	Mostly De << 1	De << 1	De << 1
Bingham number	B	$\sigma_y / \dot{\varepsilon}\eta$	Yield stress versus viscous behavior	Mostly low values (< 100)	> 1000 for crystalline	0 unless crystalline	High if slurry or cold, low otherwise	Low

TABLE 1. Definitions of parameters used in this paper and in the procedures for scaling laboratory experiments to natural lava flows.

number, the Reynolds number, the flow regime param–eter, the Deborah number, and the Bingham number.

- **Péclet number, *Pe*** – states the ratio of heat trans–fer by fluid advection to heat transfer by thermal conduction, and is expressed as UL/κ, where *U* is the mean flow velocity, *L* is a characteristic length scale (usually taken as the thickness of the flow), and κ is the thermal diffusivity of the lava. A *Pe* >>1 means that the flow is moving fast enough to advect its heat and not conduct it away. If *Pe* << 1 a flow will cool and solidify before it moves. Values of κ for natural lavas depend on the vesic–ularity [Robertson and Peck, 1974; Keszthelyi, 1994], but are usually in the range of 3–7 $\times 10^{-7}$ m²/s [e.g., Neri, 1998]. Flow speeds and thick–nesses for basaltic lava vary widely between slow moving pāhoehoe toes, where *U* =0.01–1 m/s and *L* =0.3–3 meters [Hon et al., 1994; Gregg et al., 2004]] and larger flows, with speeds of < 1 m/s for ʻaʻā and up to 20 m/s for fast channelized flows, and flow thickness of up to 20 meters [Cashman et al., 1999; Lipman and Banks, 1987]. These values

give Pe on the order of 10^{3} for a pāhoehoe toe, and on the order of 10^{8} for a channelized flow. Lava flows that have more evolved compositions are thicker and move more slowly. For example, Far–quharson et al. [2015] reported surface velocities of 3.57×10^{-5} m/s for the ≈ 30 m thick flow at Cordon–Caulle. The corresponding thermal diffusivity of a rhyolite is 5.5×10^{-7} m²/s, giving *Pe* = 1.9 x 10^{3} [Romine et al., 2012], similar to pāhoehoe toes. Hence, *Pe* for natural flows is always much greater than 1. Typical laboratory flows are thinner (0.05–0.1 meters) and slower (0.5–5 mm/s [Fink and Griffiths, 1990; Dietterich et al., 2015; Rumpf et al., 2018]). Thermal diffusivities of materials com–monly used in the laboratory range from 8.16×10^{-8} for polyethylene glycol (PEG) (Manufacturer data sheet) to 1.9×10^{-7} for corn syrup (NOAA CAMEO Chemicals website). Therefore, the *Pe* for laboratory flows is also well above 1, keeping them safely in the advection–dominated regime.

- **Reynolds number, *Re*** – measures the ratio of in–ertial forces to viscous forces in the flow, and sets

the degree to which a flow is laminar or turbulent. Re is calculated as $\rho UL/\eta$, where ρ is the fluid's density and η is the fluid's kinematic viscosity. Flow in an open channel is considered laminar for $Re < 500$ and turbulent for $Re > 2000$. With viscosities as high as 10^{10} Pa s, Re for most lava flows is typically within the laminar regime. Basalt flows, the most common low viscosity lavas, can sometimes straddle the laminar–turbulent boundary. For instance, the Re for a high–flux Hawaiian flow that is 10 meters thick, moving at 10 m/s, with a density of 2000 kg/m^3 ($\approx$30% vesicularity) and a viscosity of 100 Pa s, is 2,000, the cut–off between transitional to fully turbulent flow. Komatiite flows (viscosity of 0.1–1 Pa s) may have been fully turbulent. Because the viscosity of laboratory materials is easily controlled (for example through changes in temperature or chemical composition) they can be in either flow regime. It is important therefore to know what kind of lava flows the laboratory experiments are simulating and select the appropriate experimental parameters and material properties combination.

– **Flow regime parameter, ψ** – A popular scaling parameter for volcanological application, ψ [Fink and Griffiths, 1990; Gregg and Keszthelyi, 2004], represents the ratio between t_s, the amount of time required for a crust to form at the flow surface, and t_a, the time it takes to advect heat to a distance equivalent to the flow depth, taken as the maximum flow velocity divided by the flow depth. ψ is defined as t_s/t_a [Fink and Griffiths, 1990; Gregg and Fink, 2000; Gregg and Keszthelyi, 2004]. Values of ψ distinguish between regimes that correspond to different flow morphologies: High ψ values indicate that a flow moves faster than it has time to form a crust, and therefore the corresponding flows will have disrupted surfaces. Quantitatively, $\psi > 30$ corresponds to leveed flows and $\psi > 9$ to cracked and broken lava toes. Low ψ values, on the other hand, correlate with tube formation and inflated toes. Robertson and Kerr [2012] and Lev and James [2014] include a detailed script for calculating for both natural and laboratory flows using the material properties, flow velocity, and environmental conditions. A related characterization is given by Griffiths et al. [2003], who define the parameter $\vartheta = \Psi(R_a R_0)$, where R_a is the Rayleigh number for convection within the flow, and R_0 is taken to be equal to 100 Griffiths et al. [2003]. $\vartheta < 25$ indicates a likely development of a solid roof and a tube regime, while $\vartheta > 25$ leads to a mobile crust and an open channel flow.

– **Deborah number, De** – expresses the fluidity of a material by comparing the timescale of observation t_o with the timescale of stress relaxation t_r [Reiner, 1964]. De, defined as t_r/t_o, is relevant in particular when using non–Newtonian liquids. For a purely viscous fluid, the relaxation time is zero, and for a perfect spring, it is infinite. For a viscoelastic material (a Maxwell body) t_r is the ratio of its viscosity to Young's modulus. If the observation time is much shorter than the relaxation time ($De >> 1$), the material behaves like a solid; if the observation time is much longer, ($De << 1$) the viscous behavior dominates. For most lavas, viscous behavior dominates on the flow time and length scales, meaning De << 1. However, if the lava forms a foam, such as the case at a lava lake or a reticulite–forming fountain, viscoelasticity becomes important [Spina et al., 2016]. In addition, a viscoelastic layer is sometimes present below a solid crust at the surface of the flow [Hon et al., 1994; Lore et al., 2000; Stovall et al., 2009]. Therefore, an appropriate observation time needs to be chosen for the experiment depending on the process of interest (flow advance, crust formation, bubble coalescence...) and the chosen material.

– **Bingham number, B** – reflects the relative importance of yield stress σ_y and viscosity η for a characteristic strain rate ε: B = $\sigma_y/\varepsilon\eta$ [Griffiths, 2000]. Lavas, in particular when highly crystalline, are often considered to be Bingham or Herschel–Bulkley materials, where $\sigma_y > 0$ [McBirney and Murase, 1984]. Depending on the situation, B can be much larger or much smaller than unity. An analog material should be selected to have a similar B to that of the simulated lava system. For instance, the highly crystalline lava dome that erupted at Soufrie`re Hills, Montserrat, had a B$\approx10^4$ ([Griffiths, 2000], and a purely viscous material such as syrup would not be an appropriate analog. Instead, a clay slurry with a non–zero yield stress would be better (B for the clay–PEG slurry domes in the experiments of Griffiths and Fink [1997] was $\approx10^5$, given σ_y = 84 Pa, η=0.8 Pa s, and strain rate $\varepsilon \approx 10^3$ s^1). A large, crystal–poor,

basaltic channel flow, on the other hand, would have B << 1, and can be simulated with syrup.

2.2 MATERIALS

The choice of materials to use in a laboratory flow experiment depends on the process of interest, as well as on availability and practicality. Past laboratory flow experiments chose materials which emphasized different aspects of lava rheology, depending on the study's focus. For example, sugar–based syrups and silicone oils are simple and cheap simulants of isothermal or temperature–dependent viscous flow regimes [Dietterich et al., 2015; Garel et al., 2015]. Silicone covered in sand and flour has been used by Buisson and Merle [2005] to mimic flows with a brittle crust. Polyethylene glycol (PEG) has been used extensively to simulate solidification [e.g., Fink and Griffiths, 1990; Soule and Cashman, 2004; Garel et al., 2014; Rumpf et al., 2018], and the plastic Bingham rheology of kaoline slurries was utilized to simulate the growth of highly crystalline lava domes [Blake, 1990].

Recently, several works have negated the need to approximate lava properties with an analog by using molten basalt in large scale experiments. Currently, two US facilities, located at Syracuse University and at the University of Buffalo, perform such experiments. Lev et al. [2012] used molten basalt experiments to extract lava rheological parameters from the surface velocities of a lava flow. Edwards et al. [2013] and Oddsson et al. [2016] studied heat transfer between lava and over– or under–lying bed of ice or snow. Nonetheless, even when using molten natural rocks, there are still differences with natural lavas, for example vesicularity, crystallinity, cooling rates and crust formation.

A wealth of information exists on industrial materials that can be used for laboratory experiments, e.g. on websites, engineering handbooks, and manufacturer information sheets. One important resource is a newly developed website, a product of the European NEMOH Marie Curie Training Network. The site, located at https://sites.google.com/site/volcanologyanalogues/home, contains information about common and more unusual materials used for volcanology–related laboratory experiments, including PEG, syrup, silicone, resin, and others. While published information is essential for planning and material selection, it is important that scientists measure the properties of the actual materials they use in experiments. There can always be a "bad batch", slurries might settle, syrup might dehydrate,

PEG may have a somewhat different grade than labeled, and so on.

2.3 TOOLS AND TECHNIQUES

An experimental fluid mechanics laboratory comes with requirements, some more straight–forward than others. A water source and sink, electricity, and temperature control are needed. Other essentials include scales, heaters and freezers, thermometers/thermocouples, glassware and tanks. Windows are not desired, as external light can interfere with imaging, in particular when experiments are performed under water, as with PEG. Figure 1 shows examples of experimental environments.

Experiments require means to generate flow. Different types of fluid flow sources have been used over the years, including a dam removal (where a barrier is being removed and a reservoir spreads directly into the experiment domain, Lyman et al. [2005]; Lyman and Kerr [2006]; Applegarth et al. [2010]; Castruccio et al. [2010]), inflating a balloon inside a reservoir to push fluid out ([Blake, 1990], peristaltic pumps [e.g., Rumpf et al., 2018; Rader et al., 2017], piston–in–cylinder pumps [Griffiths and Fink, 1997; Buisson and Merle, 2005; Castruccio et al., 2014; Dietterich et al., 2015] and hydraulic squeezers [Za'vada et al., 2009].

A key component of conducting experiments is careful documentation. Cameras, both still and video, are the most common way to document experiments. Thermal infrared cameras such as FLIR (Forward–Looking Infrared) cameras are useful for collecting spatial temperature information throughout an experiment. Notable novel techniques for collecting data in laboratory experiments include sheet laser lighting [Andrews, 2014], which can see through transparent flows, and laser scanners that provide high–resolution topographic data of flow structure [Starek et al., 2011].

Data collected by cameras can be analyzed both manually and automatically using computer vision tools, to extract information about the evolution of each flow over the course of the experiments. Analysis can include tracking the flow front position and the flow width or thickness over time [e.g., Blake, 1990; Balmforth et al., 2000], as these are observables that are directly comparable with predictions from analytical or numerical models [Cordonnier et al., 2015; Dietterich et al., 2017]. A more complete dataset on the velocity distribution of the flow surface can be obtained using techniques such as Particle Image Velocimetry (PIV)
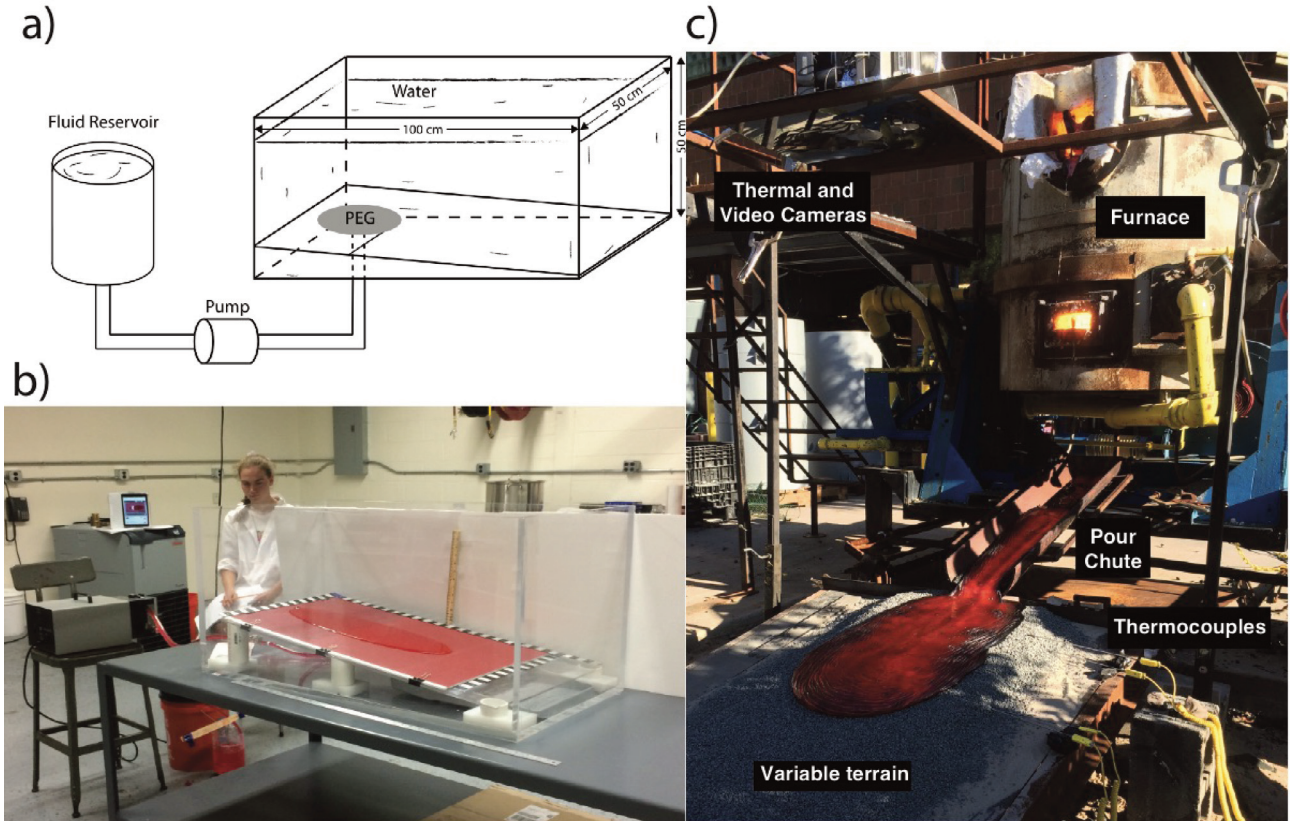
FIGURE 1. Examples of a typical analog flow experimental setup. a) The basic components of an analog experimental setup include a fluid reservoir, a pump/liquid source, a tank (with cold water in the case of PEG), and cameras and sensors to docu–ment the experiment; b) A flow experiment using corn syrup at the LDEO analog fluids lab; c) A molten basalt experi–ment at the Syracuse Lava Lab facility. A and C are from [Rumpf et al., 2018].

[e.g., Applegarth et al., 2010] or Optical Flow [e.g., Horn and Schunck, 1981; Lucas and Kanade, 1981; Lev et al., 2012]. Both techniques produce comparable results, but have different strengths and weaknesses. PIV requires that a sufficient number of seeded particles are avail–able for tracking, and care must be taken that these par–ticles do not interfere with the flow properties. The density of the particles should match that of the fluid, to prevent sinking/floating. In addition, particles em–bedded in a transparent liquid and moving towards/away from the camera may appear to be mov–ing laterally due to parallax, and thus introduce error into the measured flow field. Optical Flow assumes that the brightness of moving objects stays constant between frames. This assumption, called the "brightness con–stancy constraint" states that the brightness $I(x, y, t)$ of a pixel at position (x, y) and time t will be equal to $I(x + \partial x, y + \partial y, t + \partial t)$. These constraints translates to the so called *Optical Flow equation:* $\partial I/\partial t + \partial I/\partial x V_x + \partial I/\partial y V_y = 0$, where V_x, V_y are the velocities in the x and y directions. Because the Optical Flow equation has two unknowns, such methods require additional con–straints on the solution. These constraints can attempt, for example, to maximize the overall smoothness of the solution [Horn and Schunck, 1981], to match velocities within a certain size win– dow [Lucas and Kanade, 1981], or to use a polynomial to express the brightness in a pixel neighborhood [Farnebäck, 2003].

Photographic documentation of experiments can also yield information on flow topography and mor–phology, in addition to its kinematics. Photogrammetry techniques such as Structure–from–Motion (SfM) now provide simple and efficient means to construct high–resolution digital surface models of experimental prod–ucts through readily available software tools (e.g., Pho–toScan©, Pix4D©, and VisualSFM). The introduction of synchronized camera arrays to volcanology experi–ments [Dietterich et al., 2015; Guldstrand et al., 2018] al–lows capturing of three–dimensional flow morphology throughout the duration of an experiment, producing even more quantitative data that models should com–ply with. Figure 2 shows observations from the molten basalt obstacle experiments, including a velocity field obtained using Optical Flow (Figure 2a), a temperature

distribution as observed by a FLIR camera (Figure 2b), and a flow topography map calculated using SfM (Fig–ure 2c). An additional way to collect high–resolution to–pographic and roughness information on the flow sur–face is to use low–cost laser scanners such as the Kinect© sensor. The advances in collecting high–resolution quantitative information on flow morphology, both in the laboratory and in nature, provide a rich new dataset to compare with models.

3. THREE DECADES OF ANALOG FLOW MODELS

The field of analog laboratory experiments for lava flow studies was very active in the late 1990s and early 2000s, with the most noteworthy of those being the works by Fink and Griffiths [1990]; Fink [1992]; Fink and Griffiths [1998]; Griffiths and Fink [1997] and Sakimoto and Gregg [2001]. These early works focused on the fundamental processes of flow advance and solidifica–tion, and identified the different regimes that result from the competition between these processes. Relationships

channels resulting from levee solidification [Kerr et al., 2006].

More recent works have begun to examine more closely the impact of rheology. Robertson and Kerr [2012] built upon the studies from the 1990s and used wax–kaolin slurries to quantify the impact of non–Newtonian rheology on the solidification of a crust. Castruccio et al. [2014] looked at how flows of two–phase mixtures (sugar suspensions) behaved in a channel, and Applegarth et al. [2010] included a brittle crust at the top of their silicone–based flows. Longo et al. [2015] revisited the question of the impact of channel shapes on flow, this time using non–Newtonian materials. Other works have focused on flow cooling, particularly how it is sensed remotely by satellite or airborne thermal cameras [Garel et al., 2013, 2014; Robertson and Kerr, 2012].

Table 2 lists important experimental works from the past three decades. For each reference, the table details the materials and configuration of the experiment, its central goal, and the observable data reported in the pa–per. This table serves as a reference guide to past exper–imental works.
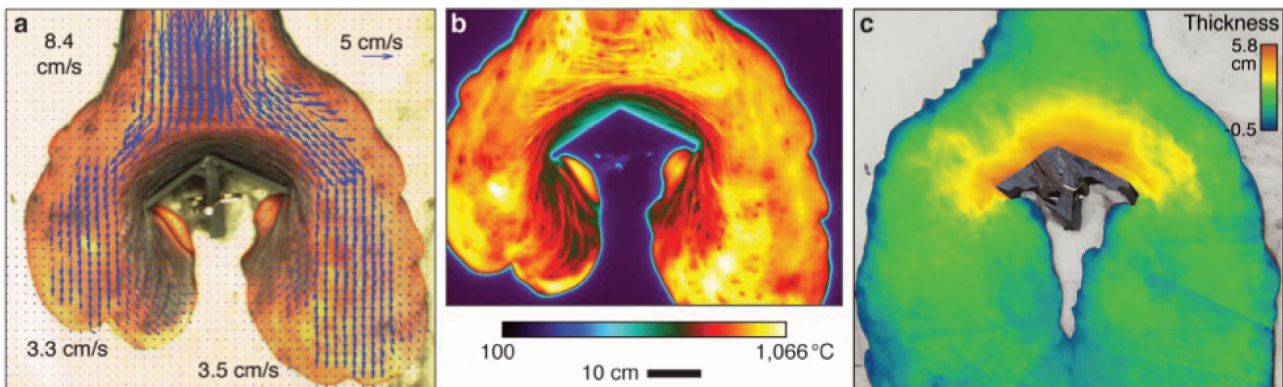

FIGURE 2. A figure by Dietterich et al. [2015], showing observations from an experiment that used molten basalt to investigate flow interaction with an obstacle. a) Visible light photo of the flow, taken from above, overlaid with arrows showing the flow's surface velocity field as analyzed by optical flow, with maximum velocities upstream and downstream of the obstacle labeled. b, Surface temperatures from the same time recorded with an overhead FLIR camera. c, Lava flow a FLIR in–frared camera from above the flow. c) Color map representing the thickness of the flow, produced by Structure–from–Motion processing of photos from a synchronized camera array.

between the rates of flow advance, effusion and cool–ing/crust formation have been defined in that time, and the impact on flow structure and morphology was rec–ognized [Balmforth et al., 2006; Blake and Bruno, 2000; Griffiths and Fink, 1997; Costa and Macedonio, 2005; Osmond and Griffiths, 2001]. In the later 2000s, empha–sis shifted to studying the impact of channels, either pre–existing channels of various shapes [Cashman et al., 2006; Takagi and Huppert, 2007, 2008] or self–forming

3.1 RECENT ADVANCES IN ANALOG LAVA FLOWS

Recently, attention has turned to using experiments to study the impact of topography of various length scales on flow evolution [Dietterich et al., 2015; Rumpf et al., 2018], perhaps in response to the ever–increas–ing availability of high–resolution topography data for volcanic regions [e.g., Deardorff and Cashman, 2012; Deligne et al., 2016]. Other recent works have looked at the effect of time variability in effusion rates [Rader et

Reference	Year	Materials used	Geometry	Goal/aim	Observables reported
Lev (This study)	2018	PEG	Unconfined, point source	Impact of slope breaks	Flow thickness Flow advance rate Flow width
Rumpf et al.	2018	Syrup, PEG, Lava	Unconfined, point source	Interaction with bed roughness	Flow front advance rate Flow thickness Flow perimeter complexity
Rader et al.	2017	PEG	Unconfined, point source	Impact of episodic effusion	Flow thickness Flow length Flow field structure
Dietterich et al.	2015	Syrup Lava	Unconfined, point source	Interaction with large obstacles	Flow front advance rate Flow thickening upslope
Long et al.	2015	Water + Glycerol / Xanthan gum	Confined, gate rise	Impact of channel shape on non-Newtonia liquid flows	Flow front advance Flow stability
Castruccio et al.	2014	Hair gel Syrup+sugar crystals	Confined, line / point source	Two-phase mixture rheology	Flow front advance rate Flow thickness
Garel et al.	2014	PEG	Unconfined, point source	Impact of cooling rate and non-constant flux	Surface temperature Flow field structure
Garel et al.	2013	Silicone oil	Unconfined, point source	Effect of wind on flow cooling	Surface temperature Flow length
Robertson and Kerr	2012	PEG+kaolin slurry (25 wt%)	Confined, gate rise	Solidification in a channel	2D surface velocity Flow thickness
Applegarth et al.	2010	Silicone and sand/plaster mixtures	Unconfined, gate rise	Effect of brittle crustal structure on flow dynamics	Flow velocity Crust structure
Castruccio et al.	2010	Syrup+sugar crystals	Confined, gate rise	Two-phase mixture rheology	Flow front advance rate Flow thickness
Kerr	2009	Solidified PEG bed and hot sucrose solution flow	Confined, point source	Thermal erosion of the bed	Bed erosion depth Bed erosion speed
Takagi and Huppert	2007	Glycerine	Confined, gate rise	Impact of channel shape	Flow front advance
Cashman et al.	2006	PEG	Confined, gate rise	Crust formation and surface morphology	Crust coverage Surface speed
Kerr et al.	2006	PEG	Unconfined, point source	Channel formation as function of flux, slope	Front advance rate Total and channel width Flow morphology
Balmforth et al.	2006	Water+kaolin slurry	Unconfined, point source	Impact of slope	Flow front advance Flow surface morphology

TABLE 2. Classic and recent references for analog experiments studying lava flow emplacement.

Reference	Year	Materials used	Geometry	Goal/aim	Observables reported
Lescinsky and Merle	2005	Silicone and sand/plaster mixtures	Confined, back push	Impact of effusion rate variations and crust rheology on flow structure	Flow surface structure Flow base structure
Sakimoto and Gregg	2001	PEG	Unconfined, point source	Flow morphology as function of flux, slope	Along and across flow velocities Flow thickness Flow width
Osmond and Griffiths	2001	PEG+kaolin slurry	Unconfined, point source	The static shape of domes	Flow volume Flow shape
Gregg and Fink	2000	PEG	Unconfined, point source	Morphology as function of slope	Flow width Flow length Flow advance rate
Blake and Bruno	2000	PEG	Unconfined, point source	Breakout timing and flow structure as function of flux and viscosity	Radius over time Time to first breakout
Griffiths and Fink	1997	PEG+kaolin slurry	Unconfined, point source	Morphology as function of flux and cooling rate	Flow width Flow morphology
Fink and Griffiths	1990	PEG	Unconfined, point source	Comparing flow morphologies from point and line sources	Flow morphology
Merle	1998	Silicone	Confined / unconfined	Internal deformation inside the flow	Internal strain within the flow Surface features (stretch, fold)

TABLE 2. Classic and recent references for analog experiments studying lava flow emplacement.

al., 2017] and of more complex rheologies [Castruccio et al., 2014; Závada et al., 2009] on flow evolution. This section highlights notable recent works as examples for the insights that volcanologists gain from laboratory experiments into outstanding questions regarding flow emplacement.

3.1.1 UNSTEADY FLOW DYNAMICS

Unsteady flow dynamics, which includes a time variable effusion of lava, lava flow inflation, and flow breakouts, are frequently observed during eruptions [e.g., Walker, 1971; Hon et al., 1994; Self et al., 1996]. However, these fundamental processes have been difficult to implement in numerical models, for instance because they require changing the computational mesh or handling a moving free surface. The physical understanding of lava flow inflation and breakouts is still lacking, and models either ignore these processes com

pletely [e.g., Harris and Rowland, 2015; Kelfoun and Vargas, 2015; Tarquini et al., 2010] or include it through a stochastic approach [Hamilton et al., 2013]. It is situations like these that analog experiments have shown their power. For example, Blake and Bruno [2000] examined the impact of flux and viscosity on the timing of breakouts.

Recent work by Rader et al. [2017] used the ability to control effusion rate provided by the laboratory setting to examine the possibility that pulsating effusion can create lava flows with wider extent than steady effusion with the same total volume production. Rader et al. [2017] used PEG and carefully calibrated effusion rates and cooling timescales to demonstrate how pulsating leads to inflation and breakout. Figure 3 (a, b) show photos of two representative experiments; the photos demonstrate the stages of inflation and the difference between steady and pulsating effusion cases. This was

a classic demonstration of the benefit of analog exper–iments to examine difficult–to–model processes. This experimental dataset will be an excellent test for future, more sophisticated flow simulation codes.

Unsteady and episodic effusion has been docu–mented repeatedly for lava domes around the world [Bluth and Rose, 2004; Harris et al., 2003; Loughlin et al., 2010; Odbert et al., 2014; Nakada et al., 1999]. Be–cause the viscous spreading timescales for domes are similar to or longer than the timescales for changes in effusion rates, time variations in effusion are likely to impact dome structure and stability. Wegleitner and Lev [2018] experimented with clay+PEG slurries and demonstrated that more episodic effusion led to rough, broken dome surfaces, compared to smooth, largely in–tact surfaces for constant effusion rates (Figure 3 c–h). This observation contributes to hazard assessment for dome collapse, since it has been shown that a dome that grows episodically and develops more damaged surface may be less stable, as well as more prone to weakening by hydrothermal alteration [Ball et al., 2013].

3.2 EXPERIMENTS ON THE IMPACT OF TOPOGRA-PHY

Lava flows naturally interact with the topography of the ground over which they are flowing. A first order parameter is the overall slope of the ground, which sets the main force driving the flow downhill. Secondary to the overall slope, several topographical factors im–pact flow evolution, including flow–scale obstacles (or, more generally, a sharp change of slope from negative to positive), small–scale variability of the ground, slope breaks (rapid steepening or shallowing of the along–flow slope) and lateral confinement by positive topog–raphy. Several recent works quantified the influence of the above factors on flow emplacement using lab ex–periments with analogs and molten basalt.

3.2.1 OBSTACLES

Many lava flows interact with steep obstacles along their path which can divert, split or confine the flow. These obstacles may be natural, such as fault scarps or a thick past flow, or human–made such as buildings. Especially in the case of buildings, such obstacles are not always large enough to be within the resolution of the digital elevation models (DEMs) used as input for flow emplacement models. Sometimes obstacles are constructed during an eruption, to divert a flow's path

away from a community or important facility [Barberi et al., 2004; Colombrita, 1984; Williams, 1983] and are thus not part of the pre–eruption DEM. However, it is important to understand how such obstacles influence flows, for instance by causing thickening upslope of the obstacle, and changing flow's advance rate [Wolfe, 1988].

Dietterich et al. [2015] showed that the orientation of a wall (linear vertical obstacle) relative to the flow direction impacts the amount of inflation behind the obstacle and the change in flow advance rate. A sim–ilar relation was observed for V–shaped obstacles, where the opening angle impacted flow thickening and speed (Figure 2). The experiments reported by Diet–terich et al. [2015] were performed using sugar syrup (a Newtonian, isoviscous fluid) and molten basalt. The re–sults from the experiments have already been used as a benchmark test to numerical flow models, as sum–marized by Dietterich et al. [2017]. Flow inflation be–hind an obstacle appeared to be a challenge for most codes tested, yet its importance cannot be overstated, especially in the context of flow hazard mitigation and flow diversion. Figure 2c shows the topography of a molten basalt flow as it thickened behind an obstacle; the topography was produced through SfM on data from an array of 10 synchronized cameras placed around the experiment ([Dietterich and Dietrich, in re–view].

Syrup and thin molten basalt experiments don't capture an important process in lava flows – the for–mation of a solid crust at the cooling flow surface above a still–molten interior. Therefore, an additional sequence of experiments was performed, using PEG. The results, shown in Figure 4, indicated that the de–gree of flow thickening above a V–shaped obstacle for all three materials used depends on the opening angle of the obstacle. The behavior of PEG was similar to that of the Newtonian isoviscous syrup, despite the forma–tion of a solid crust on the PEG flows. Basaltic flows thickened to a greater degree, pointing to a greater in–fluence of temperature–dependent viscosity compared with a solid crust. Such observations in the lab can guide priorities in improving numerical models, de–pending on the application (e.g., barrier design). Since obstacles that could be important for flows are often not represented in DEMs, models will need to include them explicitly through, perhaps, a local refinement of computational grids or a local artificial modification of the DEM.
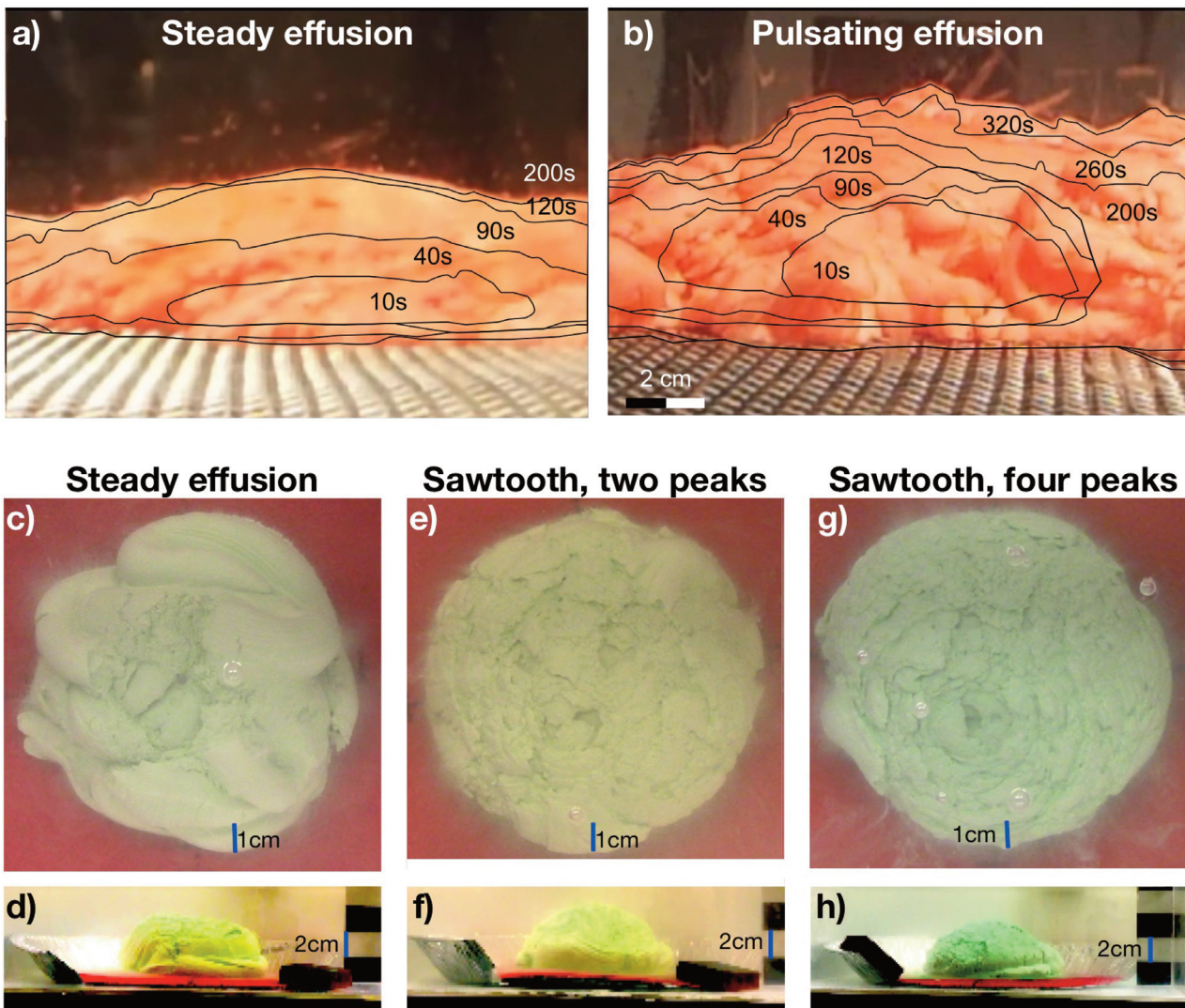
FIGURE 3. Pictures of experiments investigating the impact of pulsating effusion. Top row: Results from Rader et al., [2017]. With everything else held the same, the dome that formed by a steady, constant rate effusion (a) exhibited a smaller thick–ness and less inflation than the dome that formed by pulsating effusion (b). Center and bottom rows (c–h): Overhead and side views of products of new experiments using a clay–PEG mixture with a non–Newtonian rheology. Dome sur–face roughness and fracturing increase with increasing episodicity, from a smooth dome that formed by constant effu–sion (c, d) to rougher domes that formed by sawtooth effusion rate time sequence with two peaks (e, f) and four–peaks (g, h). The average flux for all three domes was identical.

3.2.2 SMALL-SCALE BED ROUGHNESS

At the other end of the spectrum of topographical variations, bed roughness refers to topographical vari–ations with an amplitude less than half a typical flow thickness. Anecdotal field observations from Kalauea, Hawai'i and similarly low–relief terrains indicate that the underlaying roughness impacts flows' lateral ex–tent and advance rate (and thus their cooling and morphology). Intuitively one can imagine that a flow would move slower on a rough surface. However, to date, no flow simulation code considers the influence of bed roughness on flow advancement; only topo–graphic variations large enough to be captured by the digital elevation model being used, and with the ver–tical amplitude of similar or larger to that of the typ–ical flows, are considered.

Rumpf et al. [2018] performed a series of experi–ments using corn syrup, PEG and molten basalt. Liq–uids were extruded onto substrates with amplitude–specific roughness, set by the grain size of the substrate cover material (sand, gravel, pebbles, etc). Figure 5 dis–plays overhead views of a sub–group of the experi–ments, spanning a range of bed roughness values and flow materials. The photos reveal the impact of bed roughness on flow outline complexity, with rougher (larger grain size) beds causing more irregular perime–ters and promoting breakouts. The experiments were
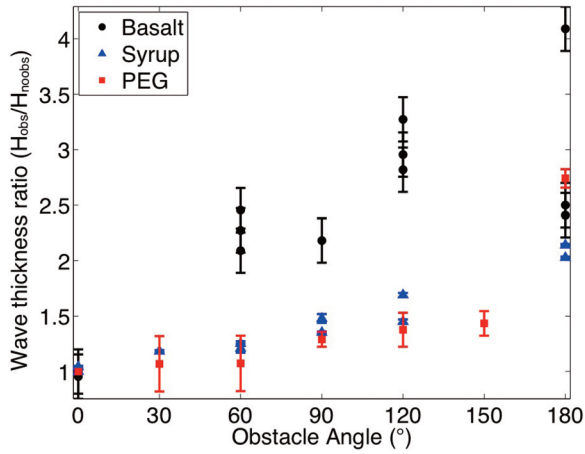
FIGURE 4. Flow thickening above a V–shaped obstacle as a function of obstacle opening angle, for three materials: Sugar syrup, PEG, and molten basalt. For all materials, flow thickens the most for an intermediate opening angle. Modified from Dietterich et al., 2015.

numerical flow models, and in particular fast probabilistic models, to incorporate information about pre–existing small–scale roughness without a significant computational cost.

3.2.3 SLOPE BREAKS

Lava flow models often calculate flow geometry (width, thickness) locally, depending on the local slope and incoming lava flux [e.g., Harris and Rowland, 2015]. However, it is possible that there might be some level of inheritance of channel structures from upslope sections to sections downslope, past a slope break [e.g., Glaze et al., 2014]. This inheritance would imply, for instance, that a flow that developed a narrow channel as it travelled on a steep slope, would be narrower than expected even at more gradual terrain. The opposite can also happen, with a flow keeping a wide cross–section despite going over a break into a steeper section. Since calculations of flow advance rate depend strongly on flow
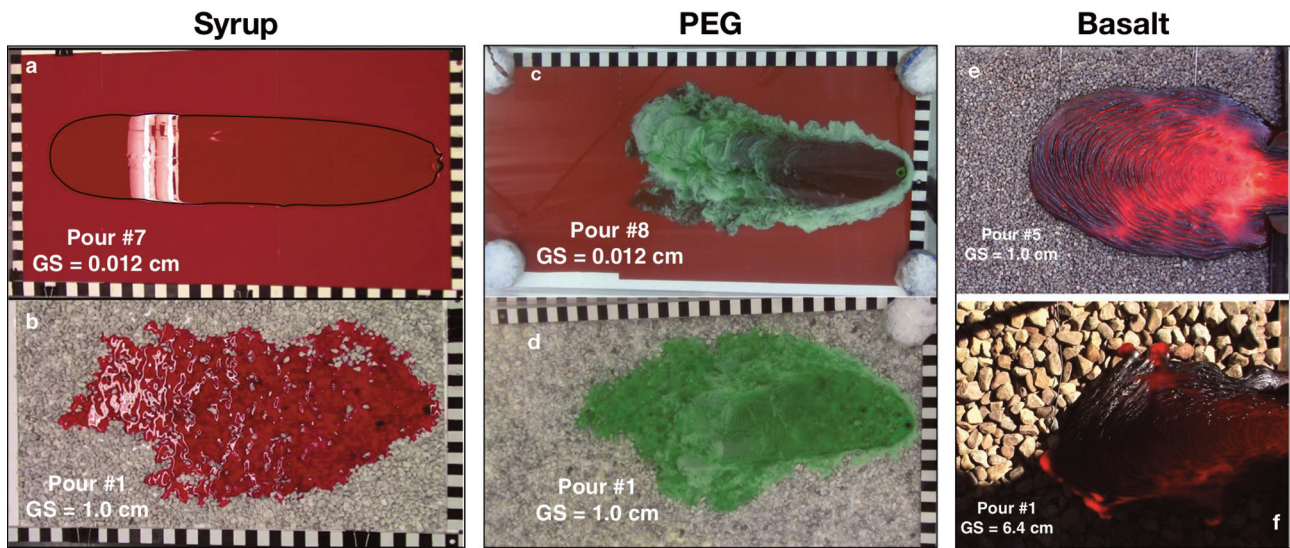

FIGURE 5. Overhead views of experiments examining the influence of bed roughness on flow emplacement. a+d: Corn syrup; b+e: PEG; c+f: Molten basalt. These photos highlight the impact of bed roughness on the morphology and perimeter geometry of the resulting flow. Beds with larger grain size (GS) lead to more irregular flow outline geometry, promoting break–outs and levee cooling. A black outline was added to panel a to mark the flow outline. Figures taken from Rumpf et al., [2018].

analyzed for flow front advance rate over time. The results, shown in Figure 6, were consistent among all three liquids tested and showed that increasing grain size led directly to a reduction in flow advance rate. The slowing down of flow advance is equivalent to an increase in the apparent viscosity of the liquid, yet the amount of that increase depended on grain size and liquid properties. The results provide a simple way for

width and thickness, it is important to capture the flow width accurately along the entire flow path. Conservation of flux through the channel would imply that a narrower–than–expected flow will advance faster than expected for its slope.

A recent sequence of experiments using syrup and PEG tested the hypothesis of flow width inheritance. Each liquid was extruded onto a slope that changed
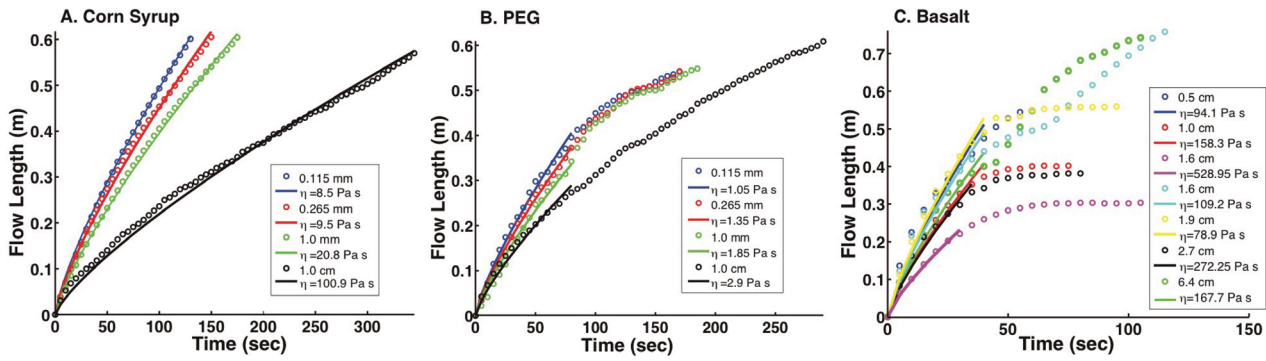
FIGURE 6. Flow front advance during analog flow experiments with varying bed roughness, from Rumpf et al., [2018]. Flow ma–terials were: A) corn syrup, B) PEG, and C) molten basalt. Circles show flow front position measured during the exper–iments. Solid curves show the best fitting analytical solution to flow advance [Lister, 1992] with a given apparent vis–cosity. Increasing roughness grain size correlates with increasing apparent viscosity.
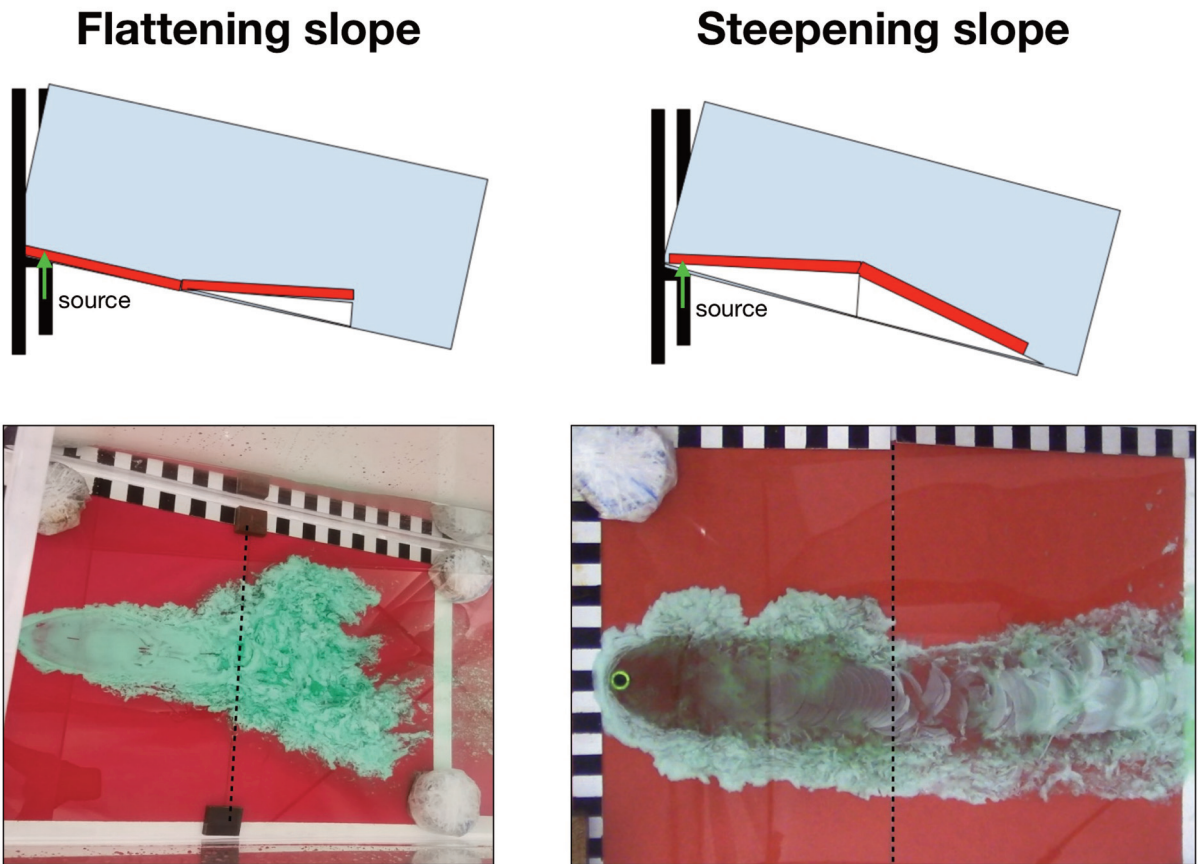

FIGURE 7. Setup schematics (top row) and overhead view of resulting flow for experiments examining the influence of slope breaks on flow width and morphology.

half–way down slope to either steeper or shallower grade. Experimental setup and overhead views of rep–resentative experiments are shown in Figure 7, and re–sults are given in Figure 8. Experiments using isoviscous syrup showed no inheritance – the flows adjusted to the new slope instantaneously at the slope break line. Flows made of PEG showed some inheritance.

If crust formation is neglected, flow front speeds should be proportional to sine of the slope at any point [Jeffreys, 1925]. For all the PEG experiments reported here, a channel forms when the flow is already in the "long–time" flow regime, dominated by downslope mo–

tion. In this situation, according to Kerr et al. [2006] (Eqn. 26 there), flow velocity U is expected to be proportional to

$$\Theta(\theta) = \left[\frac{\sin^9\theta}{\cos^6\theta}\right]^{1/13}$$

where θ is the slope. If there is no inheritance between the pre– and post–break segments, the ratio of pre– and post–break velocities should be proportional to

$$\Theta(\theta_1)/\Theta(\theta_2) = \left[\frac{\sin^9\theta_{pre}}{\cos^6\theta_{pre}}\frac{\cos^6\theta_{post}}{\sin^9\theta_{post}}\right]^{1/13}$$

As shown in Figure 8a, proximal and distal flow speeds are proportional to θ as expected, albeit with many variations. When plotting the speed ratio normalized by $\Theta(\theta_1)/\Theta(\theta_2)$ (Figure 8b), there is no systematic correlation between the ratio of proximal to distal flow speeds and the magnitude of slope break. Therefore, a steepening or shallowing of the bed does not lead to a predictable inheritance of channel structure. This finding reassures the use of models based on the local–slope.

FIGURE 8. Results of analog flow experiments using PEG on beds with slope breaks. a) Flow front advance rates as function of $\Theta(\theta) = \left[\frac{\sin^9\theta}{\cos^6\theta}\right]^{1/13}$. b) Expected flow advance rates ratio divided by $\Theta(\theta)$ as a function of the change in slope (in degrees).

4. REMAINING CHALLENGES

After many years of studying lava flows in the field, computer and laboratory, there are still many open questions, including the influence of spatial and temporal variability on the rate and extent of lava flows. As shown above, analog laboratory experiments can help scientists develop intuition and insights and construct datasets for testing simulation codes. However, several key challenges still keep us from utilizing the full power of laboratory experiments to study lava flows.

4.1 ACCESS TO 3D FLOW STRUCTURE

One current challenge is the limited ability to collect observations, either kinematic or thermal, within the interior of laboratory flows. The 3D structure of natural flows places an important control on flow behavior, as well as provides a central post–eruption observational constraint. Thus far, experimentalists are constricted to post–experiment cross–sections, which depict only the final condition and structure and no kinematic or thermal information. The three–dimensional distribution of temperature is a critical constraint on lava flow evolution, for example for determining the crust thickness and strength or the possibility of internal convection. The lack of experimental observations of the interior tem-
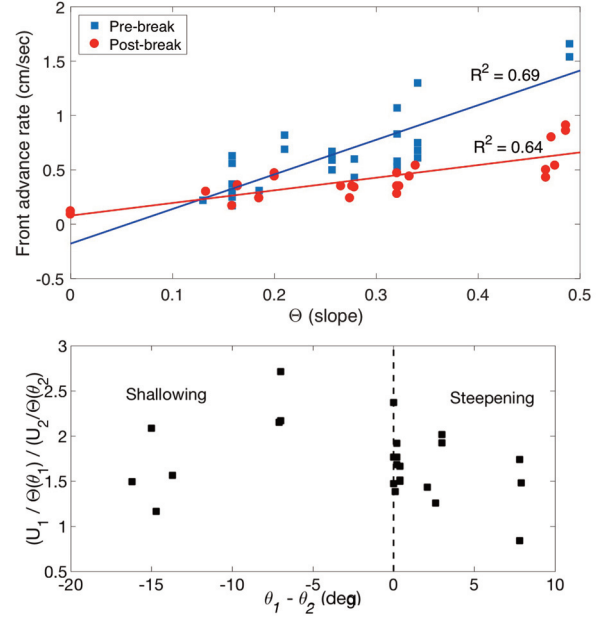
peratures within experiments inhibits testing of the accuracy of numerical flow models on this important aspect. In addition, experiments that are conducted under water, as is the case with PEG, complicate the collection of three–dimensional topography data using SfM or laser scanning, and prohibit the collection of thermal data using infrared cameras.

Potential approaches for handling the limited access to flow interior could include the use of specialty tracer particles. For example, photoelastic particles, made of certain glasses or polymers, can highlight the orientation of most compressive stress and indicate areas of high stress and strain within the flow [e.g., Estep and Dufek, 2012; Majmudar and Behringer, 2005]. Information about the 3D thermal structure of experimental flows can be revealed using thermochromatic tracers or dyes made of materials that change color as a function of temperature. For example, a leuco dye which changes color from clear to colored at a certain temperature can highlight an isotherm within the flow.

4.2 MULTIPHASE RHEOLOGY AND DYNAMICS

Another important standing challenge in the analog modeling of lava flows is capturing the complex rheology of lava flows, and in particular the influence of the multiple phases present in natural lavas. Natural

lavas contain a mix of liquid melt, solid crystals or crystal clusters, and gas bubbles, all of which influence their rheology and dynamics [Manga et al., 1998; Mader et al., 2013; Truby et al., 2015]. Replicating a similar three–phase behavior in the laboratory remains a chal–lenge. First, scaling of analog multiphase mixtures from the field to the lab is complicated by the addition of several new time and length scales. The particles and bubbles present additional length (particle and bubble size) and time (e.g., thermal conductivity or settling speed) scales to the system, as well as forces, such as surface tension or inter–particle van der Waals forces [Tsai and Zammouri, 1988]. Therefore, to ensure that the experiment resides in the same dynamic regime as the natural system, these additional scales must be considered. This is necessary, for instance, in order to avoid a situation where surface tension dominated in the lab while is negligible in nature.

Creating proper mixtures of liquids, bubbles, and particles can be technically difficult. Several recent experimental techniques show potential in this area. Centrifuges can be used to remove bubbles from a vis–cous liquid–solids mixture [e.g., Cimarelli et al., 2011]. High viscosity mixtures are more difficult to mix uni–formly. Therefore, a small number of residual bubbles is inevitable. They are often carefully mixed by hand [Cimarelli et al., 2011], but motorized mixers may pro–vide the best results. The shape of particles also has an important influence on suspension rheology [Mueller et al., 2011; Moitra and Gonnermann, 2015] and suspen–sions with different particle shapes and sizes are achieved by using, for example, rice ([Soule and Cash–man, 2005], carbon fibers [Cimarelli et al., 2011], or glass fibers [Mueller et al., 2011] for prolate solid, glit–ter [Mueller et al., 2009, 2011] for oblate particles, and crushed materials for generally angular particles [Mueller et al., 2009, 2011; Cimarelli et al., 2011].

Namiki and Manga [2008]; Oppenheimer et al. [2015] and others have used a chemical reaction of citric acid and bicarbonate of soda to produce gas bubbles within a particle suspension. Phillips et al. [1995]; Lane et al. [2001, 2008]; Mourtada–Bonnefoi and Mader [2004]; Stix and Phillips [2012]; Rivalta et al. ([2013] pro–duced bubbles by dissolving acetone in gum resin and then decompressing the material at a controlled rate. Aerators and whisks are another effective way of adding bubbles of various gases (e.g. nitrogen, air, CO2) to a suspension or a liquid [Llewellin et al., 2002; Truby et al., 2015].

New and established technologies can be utilized to characterize the mixture before, during and after ex–periments. For example, Magnetic Resonance Imaging (MRI) can image three–phase opaque mixtures in high temporal and spatial resolution and produce 3D maps of particle and bubble distribution within a sample or even a small analog flow [Tayler et al., 2012; Penn et al., 2017]. Similarly, high–rate ultrasound transducers can produce 3D maps of acoustic wave speeds within the flow, which can be calibrated to represent local density, crystallinity, vesicularity and temperature vari–ations [Ouriev and Windhab, 2002; Han et al., 2016]. Characterizing the microstructure of analog materials used in the lab is essential to allow a quantitative comparison with the microstructure found in natural lavas.

5. CONCLUSION

Experiments using analog fluids in a laboratory setting have been a critical methodology in the study of lava flows for many years, and are likely to continue being used into the future. New experimental and data collection techniques are being introduced, providing ever more data and observations. This paper presented the fundamental concepts governing experimental lava flow simulations, reviewed popular tools and methods, as well as several new works examining, for example, flow interaction with topography. Outstanding chal–lenges and potential ways to address those are dis–cussed. This summary will hopefully serve to tighten the connection between numerical modelers and experi–mentalists. A tight collaboration between experimen–talists and modelers is promised to help improve mod–els through rigorous benchmarking and evaluation, and to advance experimental techniques by defining needs and requirements.

REFERENCES

Andrews, B. J. (2014), Dispersal and air entrainment in unconfined dilute pyroclastic density currents, Bulletin of Volcanology, 76(9), 852.

Applegarth, L. J., M. R. James, B. van Wyk de Vries, and H. Pinkerton (2010), Influence of surface clinker on the crustal structures and dynamics of 'a'ā lava flows, Journal of Geophysical Research (Solid Earth), 115, B07210, doi:10.1029/2009JB006965.

Ball, J. L., E. S. Calder, B. E. Hubbard, and M. L. Bernstein (2013), An assessment of hydrothermal alteration in the Santiaguito lava dome complex, Guatemala: Implications for dome collapse hazards, Bulletin of Volcanology, 75, 676, doi:10.1007/s00445–012–0676–z.

Balmforth, N., R. Craster, A. Rust, and R. Sassi (2006), Viscoplastic flow over an inclined surface, Journal of Non–Newtonian Fluid Mechanics, 139(1–2), 103–127, doi::10.1016/j.jnnfm.2006.07.010.

Balmforth, N. J., A. S. Burbridge, R. Craster, J. Salzig, and A. Shen (2000), Visco–plastic models of isothermal lava domes, Journal of Fluid Mechanics, 403, 37–65.

Barberi, G., O. Cocina, V. Maiolino, C. Musumeci, and E. Privitera (2004), Insight into Mt. Etna (Italy) kinematics during the 2002–2003 eruption as inferred from seismic stress and strain tensors, Geophys. Res. Lett., 31, 21,614, doi:10.1029/2004GL020918.

Bilotta, G., A. Herault, A. Cappello, G. Ganci, and C. Del Negro (2016), GPUSPH: A Smoothed Particle Hydro–dynamics model for the thermal and rheological evolution of lava flows, Geological Society of London Special Publications, 426, 387–408, doi:10.1144/SP426.24.

Blake, S. (1990), Viscoplastic models of lava domes, in Lava flows and domes, pp. 88–126, Springer.

Blake, S., and B. C. Bruno (2000), Modelling the emplacement of compound lava flows, Earth and Planetary Science Letters, 184, 181–197, doi:10.1016/S0012–821X(00)00278–8.

Bluth, G. J., and W. I. Rose (2004), Observations of eruptive activity at Santiaguito volcano,Gguatemala, Journal of Volcanology and Geothermal research, 136(3), 297–302.

Buckingham, E. (1914), On physically similar systems; illustrations of the use of dimensional equations, Physical review, 4(4), 345.

Buisson, C., and O. Merle (2005), Influence of crust thickness on dome destabilization, Geological Society of America Special Papers, 396, 181–188.

Cappello, A., A. He ₽ault, G. Bilotta, G. Ganci, and C. Del Negro (2015), MAGFLOW: A physics–based model for the dynamics of lava–flow emplacement, Geological Society, London, Special Publications, 426, SP426–16.

Cashman, K. V., C. Thornber, and J. P. Kauahikaua (1999), Cooling and crystallization of lava in open channels, and the transition of Pāhoehoe Lava to 'A'ā, Bull. Volcanol., 61, 306–323, doi:10.1007/s004450050299.

Cashman, K. V., R. C. Kerr, and R. W. Griffiths (2006), A laboratory model of surface crust formation and disruption on lava flows through non–uniform channels, Bull. Volcanol., 68, 753–770, doi:10.1007/s00445–005–0048–z.

Castruccio, A., A. C. Rust, and R. S. J. Sparks (2010), Rheology and flow of crystal–bearing lavas: Insights from analogue gravity currents, Earth and Planetary Science Letters, 297, 471–480, doi:10.1016/j.epsl.2010.06.051.

Castruccio, A., A. C. Rust, and R. S. J. Sparks (2014), Assessing lava flow evolution from post–eruption field data using Herschel–Bulkley rheology, Journal of Volcanology and Geothermal Research, 275, 71–84, doi:10.1016/j. jvolgeores.2014.02.004.

Cimarelli, C., A. Costa, S. Mueller, and H. M. Mader (2011), Rheology of magmas with bimodal crystal size and shape distributions: Insights from analog experiments, Geochemistry, Geophysics, Geosystems, 12(7).

Colombrita, R. (1984), Methodology for the construction of earth barriers to divert lava flows: The Mt. Etna 1983 eruption, Bull. Volcanol., 47, 1009–1038, doi:10.1007/BF01952358.

Cordonnier, B., E. Lev, and F. Garel (2015), Benchmarking lava–flow models, Geological Society, London, Special Publications, 426, doi:10.1144/SP426.7.

Costa, A., and G. Macedonio (2005), Extensional and compressional strain in lava flows and the formation of fractures in surface crust, in Kinematics and dynamics of lava flows, edited by M. Manga and G. Ventura, p. 163, Geological Society of America, Special Paper 396.

Deardorff, N. D., and K. V. Cashman (2012), Emplacement conditions of the c. 1,600–year bp Collier

Cone lava flow, Oregon: A LiDAR investigation, Bulletin of Volcanology, 74, 2051–2066, doi:10.1007/s00445–012–0650–9.

Deligne, N. I., R. M. Conrey, K. V. Cashman, D. E. Champion, and W. H. Amidon (2016), Holocene volcanism of the upper McKenzie river catchment, central Oregon Cascades, USA, Bulletin, 128(11–12), 1618–1635.

Dietterich, H. R., and J. Dietrich (in review), 4d imaging of lava flows in the lab, Geophysical Research Letters.

Dietterich, H. R., K. V. Cashman, A. C. Rust, and E. Lev (2015), Diverting lava flows in the lab, Nature Geoscience, 8, 494–496, doi:10.1038/ngeo2470.

Dietterich, H. R., E. Lev, J. Chen, J. A. Richardson, and K. V. Cashman (2017), Benchmarking computational fluid dynamics models of lava flow simulation for hazard assessment, forecasting, and risk management, Journal of Applied Volcanology, 6(1), 9.

Edwards, B. R., J. Karson, R. Wysocki, E. Lev, I. Bindeman, and U. Kueppers (2013), Insights on lava–ice/snow interactions from large–scale basaltic melt experiments, Geology, 41, 851–854, doi:10.1130/G34305.1.

Estep, J., and J. Dufek (2012), Substrate effects from force chain dynamics in dense granular flows, Journal of Geophysical Research (Earth Surface), 117, F01028, doi:10.1029/2011JF002125.

Farnebäck, G. (2003), Two–frame motion estimation based on polynomial expansion, in Scandinavian conference on Image analysis, pp. 363–370, Springer.

Farquharson, J., M. James, and H. Tuffen (2015), Examining rhyolite lava flow dynamics through photo–based 3d reconstructions of the 2011–2012 lava flow field at cordo'n–caulle, chile, Journal of Volcanology and Geothermal Research, 304, 336–348.

Fink, J. (1992), A laboratory analog study of the surface morphology of lava flows extruded from point and line sources, J. Volcanol. Geotherm. Res., 54, 19–32, doi:10.1016/0377–0273(92)90112–Q.

Fink, J. H., and R. W. Griffiths (1990), Radial spreading of viscous–gravity currents with solidifying crust, Journal of Fluid Mechanics, 221, 485–509, doi:10.1017/S0022112090003640.

Fink, J. H., and R. W. Griffiths (1998), Morphology, eruption rates, and rheology of lava domes: Insights from laboratory models, Journal of Geo-

physical Research: Solid Earth (1978–2012), 103(B1), 527–545.

Garel, F., E. Kaminski, S. Tait, and A. Limare (2013), The influence of wind on the estimation of lava effusion rate from thermal remote–sensing, Journal of Volcanology and Geothermal Research, 264, 223–230, doi:10.1016/j. jvolgeores.2013.08.006.

Garel, F., E. Kaminski, S. Tait, and A. Limare (2014), An analogue study of the influence of solidification on the advance and surface thermal signature of lava flows, Earth and Planetary Science Letters, 396, 46–55, doi:10. 1016/j.epsl.2014.03.061.

Garel, F., E. Kaminski, S. Tait, and A. Limare (2015), A fluid dynamics perspective on the interpretation of the surface thermal signal of lava flows, Geological Society, London, Special Publications, 426, SP426–6.

Glaze, L. S., Baloga, S. M., Fagents, S. A., & Wright, R. (2014). The influence of slope breaks on lava flow surface disruption. Journal of Geophysical Research: Solid Earth, 119(3), 1837–1850.

Gregg, C. E., B. F. Houghton, D. M. Johnston, D. Paton, and D. A. Swanson (2004), The perception of volcanic risk in Kona communities from Mauna Loa and Hualalai volcanoes, Hawai'i, J. Volcanol. Geotherm. Res., 130, 179–196, doi:10.1016/S0377–0273(03)00288–9.

Gregg, T. K. P., and J. H. Fink (2000), A laboratory investigation into the effects of slope on lava flow morphology, J. Volcanol. Geotherm. Res., 96, 145–159, doi:10.1016/S0377–0273(99)00148–1.

Gregg, T. K. P., and L. P. Keszthelyi (2004), The emplacement of pāhoehoe toes: Field observations and comparison to laboratory simulations, Bull. Volcanol., 66, 381–391, doi:10.1007/s00445–003–0319–5.

Griffiths, R. W. (2000), The Dynamics of Lava Flows, Annual Review of Fluid Mechanics, 32, 477–518, doi:10.1146/ annurev.fluid.32.1.477.

Griffiths, R. W., and J. H. Fink (1997), Solidifying Bingham extrusions: A model for the growth of silicic lava domes, Journal of Fluid Mechanics, 347, 13–36.

Griffiths, R. W., R. C. Kerr, and K. V. Cashman (2003), Patterns of solidification in channel flows with surface cooling, Journal of Fluid Mechanics, 496, 33–62, doi:10.1017/S0022112003006517.

Guldstrand, F., O. Galland, E. Hallot, and S. Burchardt

(2018), Experimental constraints on forecasting the location of volcanic eruptions from pre-eruptive surface deformation, Frontiers in Earth Science, 6, 7.

Hamilton, C. W., L. S. Glaze, M. R. James, and S. M. Baloga (2013), Topographic and stochastic influences on pāhoehoe lava lobe emplacement, Bulletin of Volcanology, 75, 756, doi:10.1007/s00445-013-0756-8.

Han, E., I. R. Peters, and H. M. Jaeger (2016), High-speed ultrasound imaging in dense suspensions reveals impact–activated solidification due to dynamic shear jamming, Nature communications, 7, 12,243.

Harris, A. J., and S. K. Rowland (2015), Flowgo 2012: An updated framework for thermorheological simulations of channel–contained lava, Hawaiian Volcanoes: From Source to Surface, 208, 457.

Harris, A. J., W. I. Rose, and L. P. Flynn (2003), Temporal trends in lava dome extrusion at santiaguito 1922–2000, Bulletin of Volcanology, 65(2–3), 77–89.

Harris, A. J., T. De Groeve, F. Garel, and S. A. Carn (2016), Detecting, modelling and responding to effusive eruptions, Geological Society of London.

Harris, A. J. L., M. Rhety, L. Gurioli, N. Villeneuve, and R. Paris (2016), Simulating the thermorheological evolution of channel–contained lava: FLOWGO and its implementation in EXCEL, Geological Society of London Special Publications, 426, 313–336, doi:10.1144/SP426.9.

Head, J. W., L. Crumpler, J. C. Aubele, J. E. Guest, and R. S. Saunders (1992), Venus volcanism: Classification of volcanic features and structures, associations, and global distribution from magellan data, Journal of Geophysical Research: Planets, 97(E8), 13,153–13,197.

Hidaka, M., A. Goto, S. Umino, and E. Fujita (2005), VTFS project: Development of the lava flow simulation code LavaSIM with a model for three–dimensional convection, spreading, and solidification, Geochem. Geophys. Geosys., 6, Q07,008, doi:10.1029/2004GC000869.

Hon, K., J. Kauahikaua, R. Denlinger, and K. Mackay (1994), Emplacement and inflation of pāhoehoe sheet flows: Observations and measurements of active lava flows on kilauea volcano, hawaii, Geological Society of America Bulletin, 106(3), 351–370.

Horn, B. K., and B. G. Schunck (1981), Determining op-

tical flow, Artificial Intelligence, 17, 185–203.

Jeffreys, H. (1925), Lxxxiv. the flow of water in an inclined channel of rectangular section, The London, Edinburgh, and Dublin Philosophical Magazine and Journal of Science, 49(293), 793–807.

Jenkins, S. F., S. Day, B. Faria, and J. Fonseca (2017), Damage from lava flows: Insights from the 2014–2015 eruption of Fogo, Cape Verde, Journal of Applied Volcanology, 6(1), 6.

Kavanagh, J. L., S. L. Engwell, and S. A. Martin (2018), A review of laboratory and numerical modelling in volcanology, Solid Earth, 9(2), 531–571.

Kelfoun, K., and S. V. Vargas (2015), Volcflow capabilities and potential development for the simulation of lava flows, Geological Society, London, Special Publications, 426, SP426-8.

Kerr, R. C., R. W. Griffiths, and K. V. Cashman (2006), Formation of channelized lava flows on an unconfined slope, J. Geophys. Res., 111(B10), B10,206, doi:10.1029/2005JB004225.

Keszthelyi, L. (1994), Calculated effect of vesicles on the thermal properties of cooling basaltic lava flows, Journal of Volcanology and Geothermal Research, 63(3–4), 257–266.

Lane, S. J., B. A. Chouet, J. C. Phillips, P. Dawson, G. A. Ryan, and E. Hurst (2001), Experimental observations of pressure oscillations and flow regimes in an analogue volcanic system, Journal of Geophysical Research: Solid Earth, 106(B4), 6461–6476.

Lane, S. J., J. Phillips, and G. Ryan (2008), Dome-building eruptions: Insights from analogue experiments, Geological Society, London, Special Publications, 307(1), 207–237.

Lev, E., and M. R. James (2014), The influence of cross-sectional channel geometry on rheology and flux estimates for active lava flows, Bulletin of Volcanology, 76, 829, doi:10.1007/s00445-014-0829-3.

Lev, E., M. Spiegelman, R. J. Wysocki, and J. A. Karson (2012), Investigating lava flow rheology using video analysis and numerical flow models, Journal of Volcanology and Geothermal Research, 247, 62–73, doi:10.1016/j. jvolgeores.2012.08.002.

Lipman, P. W., and N. G. Banks (1987), AA flow dynamics, Mauna Loa 1984, in Volcanism in Hawaii. US Geological Survey Professional Paper, vol. 1350, edited by R. W. Decker, T. L. Wright, and P. H. Stauffer, pp. 1527–1567.

Lister, J. R. (1992), Viscous flows down an inclined plane from point and line sources, Journal of Fluid Mechanics, 242, 631–653.

Llewellin, E., H. Mader, and S. Wilson (2002), The constitutive equation and flow dynamics of bubbly magmas, Geophysical research letters, 29(24).

Longo, S., V. Di Federico, and L. Chiapponi (2015), Non–Newtonian power–law gravity currents propagating in confining boundaries, Environmental Fluid Mechanics, 15(3), 515–535.

Lore, J., H. Gao, and A. Aydin (2000), Viscoelastic thermal stress in cooling basalt flows, J. Geophys. Res., 105, 23,695–23,710, doi:10.1029/2000JB900226.

Loughlin, S., R. Luckett, G. Ryan, T. Christopher, V. Hards, S. De Angelis, L. Jones, and M. Strutt (2010), An overview of lava dome evolution, dome collapse and cyclicity at Soufrie`re Hills volcano, Montserrat, 2005–2007, Geophysical Research Letters, 37(19).

Lucas, B. D., and T. Kanade (1981), An iterative image registration technique with an application to stereo vision, in Proceedings of Imaging Understanding Workshop, pp. 121–130.

Lyman, A. W., and R. C. Kerr (2006), Effect of surface solidification on the emplacement of lava flows on a slope, J. Geophys. Res., 111(b10), 5206, doi:10.1029/2005JB004133.

Lyman, A. W., R. C. Kerr, and R. W. Griffiths (2005), Effects of internal rheology and surface cooling on the emplacement of lava flows, J. Geophys. Res., 110(b9), 8207, doi:10.1029/2005JB003643.

Mader, H., E. Llewellin, and S. Mueller (2013), The rheology of two–phase magmas: A review and analysis, Journal of Volcanology and Geothermal Research, 257, 135–158.

Majmudar, T. S., and R. P. Behringer (2005), Contact force measurements and stress–induced anisotropy in granular materials, Nature, 435(7045), 1079.

Manga, M., and G. Ventura (2005), Kinematics and dynamics of lava flows, vol. 396, Geological Society of America. Manga, M., J. Castro, K. Cashman, and M. Loewenberg (1998), Rheology of bubble–bearing magmas, J. Volcanol. Geotherm. Res., 87, 15–28.

McBirney, A., and T. Murase (1984), Rheological properties of magmas, Annual Review of Earth and Planetary Sciences, 12(1), 337–357.

Merle, O. (2015), The scaling of experiments on vol–

canic systems, Frontiers in Earth Science, 3, 26.

Moitra, P., and H. Gonnermann (2015), Effects of crystal shape–and size–modality on magma rheology, Geochemistry, Geophysics, Geosystems, 16(1), 1–26.

Mourtada–Bonnefoi, C., and H. Mader (2004), Experimental observations of the effect of crystals and pre–existing bubbles on the dynamics and fragmentation of vesiculating flows, Journal of Volcanology and Geothermal Research, 129(1–3), 83–97.

Mueller, S., H. Mader, and E. Llewellin (2009), Crystals in magma: Flow dynamics and rheology of particle–bearing melts, in EGU General Assembly Conference Abstracts, vol. 11, p. 8774.

Mueller, S., E. Llewellin, and H. Mader (2011), The effect of particle shape on suspension viscosity and implications for magmatic flows, Geophysical Research Letters, 38(13).

Nakada, S., H. Shimizu, and K. Ohta (1999), Overview of the 1990–1995 eruption at Unzen volcano, Journal of Volcanology and Geothermal Research, 89(1), 1–22.

Namiki, A., and M. Manga (2008), Transition between fragmentation and permeable outgassing of low viscosity magmas, Journal of Volcanology and Geothermal Research, 169(1–2), 48–60.

Neri, A. (1998), A local heat transfer analysis of lava cooling in the atmosphere: Application to thermal diffusion–dominated lava flows, Journal of Volcanology and Geothermal Research, 81(3–4), 215–243.

Odbert, H. M., R. C. Stewart, and G. Wadge (2014), Cyclic phenomena at the soufrie`re hills volcano, montserrat, Geological Society, London, Memoirs, 39(1), 41–60.

Oddsson, B., M. T. Gudmundsson, I. Sonder, B. Zimanowski, and A. Schmid (2016), Experimental studies of heat transfer at the dynamic magma ice/water interface: Application to subglacially emplaced lava, Journal of Geophysical Research (Solid Earth), 121, 3261–3277, doi:10.1002/2016JB012865.

Oppenheimer, J., Rust, A. C., Cashman, K. V., & Sandnes, B. (2015). Gas migration regimes and outgassing in particle–rich suspensions. Frontiers in Physics, 3, 60.

Osmond, D. I., and R. W. Griffiths (2001), The static shape of yield strength fluids slowly emplaced on slopes, J. Geophys. Res., 106, 16,241–16,250, doi:10.1029/2001JB000405.

Ouriev, B., and E. Windhab (2002), Novel ultrasound–based time averaged flow mapping method for die entry visualization in flow of highly concentrated shear–thinning and shear–thickening suspensions, Measurement Science and Technology, 14(1), 140.

Patrick, M., T. Orr, G. Fisher, F. Trusdell, and J. Kauahikaua (2017), Thermal mapping of a pāhoe–hoe lava flow, kā lauea volcano, Journal of Volcanology and Geothermal Research, 332, 71–87.

Penn, A., T. Tsuji, D. O. Brunner, C. M. Boyce, K. P. Pruessmann, and C. R. Mu ̈ler (2017), Real–time probing of granular dynamics with magnetic resonance, Science Advances, 3(9), e1701,879.

Phillips, J., S. Lane, A.–M. Lejeune, and M. Hilton (1995), Gum rosin–acetone system as an analogue to the degassing behaviour of hydrated magmas, Bulletin of Volcanology, 57(4), 263–268.

Rader, E., L. Vanderkluysen, and A. Clarke (2017), The role of unsteady effusion rates on inflation in long–lived lava flow fields, Earth and Planetary Science Letters, 477, 73–83.

Reiner, M. (1964), The deborah number, Physics today, 17(1), 62.

Rivalta, E., K. Pascal, J. Phillips, and A. Bonaccorso (2013), Explosive expansion of a slowly decompressed magma analogue: Evidence for delayed bubble nucleation, Geochemistry, Geophysics, Geosystems, 14(8), 3067–3084.

Robertson, E. C., and D. L. Peck (1974), Thermal conductivity of vesicular basalt from Hawai'i, Journal of Geophysical Research, 79(32), 4875–4888.

Robertson, J., and R. Kerr (2012), Solidification dynamics in channeled viscoplastic lava flows, J. Geophys. Res., 117(B7), B07,206, doi:10.1029/2012JB00916.

Romine, W. L., A. G. Whittington, P. I. Nabelek, and A. M. Hofmeister (2012), Thermal diffusivity of rhyolitic glasses and melts: Effects of temperature, crystals and dissolved water, Bulletin of volcanology, 74(10), 2273–2287.

Rumpf, M. E., E. Lev, and R. Wysocki (2018), The influence of topographic roughness on lava flow emplacement, Bull. Volc., in press.

Sakimoto, S. E. H., and T. K. P. Gregg (2001), Channeled flow: Analytic solutions, laboratory experiments, and applications to lava flows, ournal of Geophysical Research, 106, 8629–8644, doi:10.1029/2000JB900384.

Self, S., T. Thordarson, L. Keszthelyi, G. P. L. Walker, K. Hon, M. T. Murphy, P. Long, and S. Finnemore (1996), A new model for the emplacement of Columbia River basalts as large, inflated pahoe–hoe lava flow fields, Geophys. Res. Lett., 23, 2689–2692, doi:10.1029/96GL02450.

Soule, S. A., and K. V. Cashman (2004), The mechanical properties of solidified polyethylene glycol 600, an analog for lava crust, J. Volcanol. Geotherm. Res., 129(1–3), 139–153.

Soule, S. A., and K. V. Cashman (2005), Shear rate dependence of the pāhoehoe–to–a'a transition: Analog experiments, Geology, 33, 361, doi:10.1130/G21269.1.

Spina, L., B. Scheu, C. Cimarelli, A. Arciniega–Ceballos, and D. Dingwell (2016), Time scales of foam stability in shallow conduits: Insights from analogue experiments, Geochemistry, Geophysics, Geosystems, 17(10), 4179– 4194.

Starek, M. J., H. Mitasova, E. Hardin, K. Weaver, M. Overton, and R. S. Harmon (2011), Modeling and analysis of landscape evolution using airborne, terrestrial, and laboratory laser scanning, Geosphere, 7(6), 1340–1356.

Stix, J., and J. C. Phillips (2012), An analog investigation of magma fragmentation and degassing: Effects of pressure, volatile content, and decompression rate, Journal of Volcanology and Geothermal Research, 211, 12–23.

Stovall, W. K., B. F. Houghton, A. J. L. Harris, and D. A. Swanson (2009), Features of lava lake filling and draining and their implications for eruption dynamics, Bull. Volcanol., 71, 767–780, doi:10.1007/s00445–009–0263–0.

Takagi, D., and H. E. Huppert (2007), The effect of confining boundaries on viscous gravity currents, Journal of Fluid Mechanics, 577(1), 495–505.

Takagi, D., and H. E. Huppert (2008), Viscous gravity currents inside confining channels and fractures, Physics of Fluids, 20(2), 495–505, doi:10.1063/1.2883991.

Tarquini, S., M. Favalli, and A. Fornaciai (2010), Lava flow hazard and risk maps using DOWNFLOW: Sensitivity analysis and maps updating, EGU General Assembly 2010, held 2–7 May, 2010 in Vienna, Austria, p.8397, 12, 8397.

Tayler, A. B., D. J. Holland, A. J. Sederman, and L. F. Gladden (2012), Exploring the origins of turbulence in multi–phase flow using compressed

sensing mri, Physical review letters, 108(26), 264,505.

Truby, J., S. Mueller, E. Llewellin, and H. Mader (2015), The rheology of three–phase suspensions at low bubble capillary number, in Proc. R. Soc. A, vol. 471(2173), p. 20140557, The Royal Society.

Tsai, S. C., and K. Zammouri (1988), Role of interpar–ticular van der Waals force in rheology of con–centrated suspensions, Journal of Rheology, 32(7), 737–750.

Walker, G. (1971), Compound and simple lava flows and flood basalts, Bulletin Volcanologique, 35(3), 579–590. Wegleitner, K. A., and E. Lev (2018), In–vestigating the effect of viscosity and pulsating effusion rates on lava dome morphology through physical models, AGU Fall Meeting, V23F–0137.

Williams, S. N. (1983), Plinian airfall deposits of basaltic composition, Geology, 11(4), 211–214.

Wilson, L., and J. W. Head (1983), A comparison of volcanic eruption processes on earth, moon, mars, io and Venus, Nature, 302(5910), 663.

Wolfe, E. W. (1988), The puu oo eruption of kilauea volcano, hawaii: Episode 1 through 20, january 3, 1983, through june 8, 1984., US Geol. Serv. Prof. Paper, 1463, 251p.

Za'vada, P., Z. Kratinova', V. Kusbach, and K. Schul–mann (2009), Internal fabric development in complex lava domes, Tectonophysics, 466(1), 101–113.

*CORRESPONDING AUTHOR:Einat LEV,

Lamont-Doherty Earth Observatory,

Columbia University,

New-York, NY,

USA

email: einatlev@ldeo.columbia.com